Analysis of Transmission Lines of Finite Thickness Above a Periodically Perforated Ground Plane at Oblique Orientations

Guangwen Pan, *Senior Member, IEEE*, Xiaojun Zhu, *Student Member IEEE*, and Barry K. Gilbert, *Senior Member, IEEE*

***Abstract*—A general method is formulated for the analysis of signal lines of finite thickness in the presence of a periodically perforated ground plane. Utilizing the dyadic Green's functions, a set of electric and magnetic field integral equations (EFIE, MFIE) is established, which are then transformed into the spectral domain by the Fourier transform. Galerkin's method is used to solve the combined integral equations. The B-spline functions are chosen as basis functions to achieve a higher order of convergence. The dispersive characteristics of the transmission lines are studied and the characteristic impedance of the signal lines are evaluated by both the voltage-current definition and the power-current definition, with good consistency. The effect of signal locations versus apertures in the ground plane is discussed. Finally, measurements are conducted, and the results agreed very well with the theory.**

I. Introduction

PERIODICALLY perforated conductor screens have become an important part of modern microelectronic packaging. In particular, the so-called deposited metal-organic multichip modules (MCM-Ds), which represent the newest electronic packaging technology for high performance digital processors, typically are fabricated with meshed rather than solid power and ground planes [1].

The modeling and simulation of electromagnetic performance for modern packaging with solid ground plane(s) have been studied by the quasi-static and full-wave approaches [2]–[5], while the propagation characteristics of a signal line above a periodically perforated ground have previously been studied [6]–[8].

In [6], the relationship between the fields and the electric current is derived from the boundary condition under the assumption of infinitesimally thin conductors, and the periodicity of the structure is taken into account by using the Floquet principle. Using a similar method, Chan *et al.* [8] studied the case in which the signal lines are in a multilayered medium. In both cases the apertures are rectangular, the signal lines are parallel to the edge of the apertures, and the conductors are assumed to be of zero thickness; both methods employed EFIE formulation.

One disadvantage of the EFIE formulation is that in order to find the solution, the electric current on all conductors needs to be solved, which results in a large matrix and requires substantial computing resources. When the structure is very complicated, it is impractical to use this method due to the complexity of the current distribution, and the slow convergence of the double Fourier series.

In this paper, a set of surface EFIEs and surface MFIEs are derived by imposing the dyadic Green's functions. The periodic system is obtained by finding the Fourier transforms of the field and current distributions. The contribution of the meshed ground plane is taken into account by the magnetic current and the images of the signal lines. Thus, a combined EFIE and MFIE method is formulated. These integral equations are then converted into a set of matrix equations using Galerkin's method, and an eigenvalue problem is established. Solving the eigensystem, all the working modes of the system are obtained.

Once the eigensolution is attained, the characteristic impedance of the signal lines is evaluated by the voltage-current definition and the power-current definition. It is shown that the characteristic impedance is a constant along the signal direction. This finding is very much in contradiction to the conventional concept and the results given by [9], in which the impedance of the signal line is larger above the apertures than that above the ground metal.

One important factor in Galerkin's solution is the choice of the basis functions. Since the convergence of the double Fourier series depends upon the smoothness of the basis, a carefully chosen basis may speed up the rate of convergence significantly. In this paper, the B-spline functions of different orders will be used as basis functions.

The periodic apertures make the system behave as a slow wave structure, which is undesirable in the high speed circuitry. As a result, we focus on the characteristic impedance and the dispersive behavior of the signal lines, which are affected by the shape, size and orientation of the apertures, as well as by the relative locations of the signal lines to the apertures as will be seen in Table I of Section IV. This slow wave phenomenon was not detected by the FDTD method (Table IV, [11]). Finally, we present the results of

Manuscript received August 28, 1993; revised March 28, 1994. This research is supported in part by ARPA/ESTO under Contract N00014-91-J-4030 from the Office of Naval Research, and Contract 133-P771 from Boeing Aerospace Corporation.

G. Pan is with the Signal Propagation Research Laboratory, Dept. of EE&CS, University of Wisconsin-Milwaukee, Milwaukee, WI 53201 USA.

X. Zhu is with Ansoft Corp., Pittsburgh, PA 15219 USA.

B. Gilbert is with the Department of Physiology and Biophysics, Mayo Foundation, Rochester, MN 55905 USA.

IEEE Log Number 9407291.

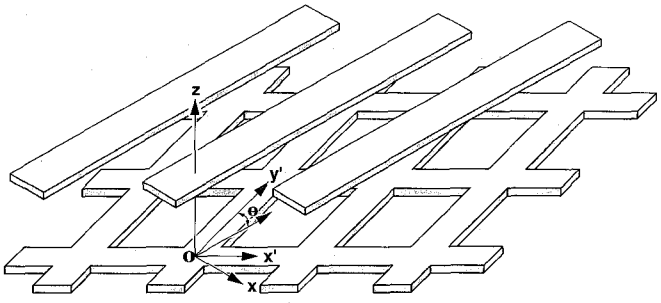

Fig. 1. Two-dimensional periodic structure.

measurement conducted on a test coupon, with the theoretical results compared with the measurements.

The remainder of this paper is arranged as follows: Section II provides the basic formulation of the method, in which a detailed derivation of the integral equations based on the equivalence principle and dyadic Green's functions is presented. Section III discusses the choice of the basis functions and presents the Galerkin's solution for the cases where the signal lines are oriented arbitrarily. Section IV compares the two definitions of the characteristic impedance. Section V presents the numerical results and comparisons. A conclusion is presented in Section V.

II. General Formulation

In this section, we shall derive the combined field integral equations for a strip line above a perforated ground plane by means of the equivalence principle and dyadic Green's functions.

A. Equivalence Principle and Integral Equations

A general structure of the system is shown in Fig. 1 in which the shape of the apertures can be arbitrary, as long as the configuration is periodic. Employing the boundary condition, we obtain the EFIE as

$$\mathbf{E}_e(\mathbf{r}) \times \hat{\mathbf{n}} = 0 \tag{1}$$

where $\mathbf{E}_e(\mathbf{r})$ denotes the electric field induced by the electric current. Using the dyadic Green's function, we have

$$\mathbf{E}_e(\mathbf{r}) = -j\omega\mu \int \bar{\mathbf{G}}_{Ee}(\mathbf{r},\mathbf{r}') \cdot \mathbf{J}(\mathbf{r}')dv' \tag{2}$$

In the previous equation $\mathbf{r} \in S$, the surface of the conductors, and $\bar{\mathbf{G}}_{Ee}(\mathbf{r},\mathbf{r}')$ is the dyadic Green's function, which will be given later. The EFIE approach requires the electric current on all conductor surfaces including signals and ground planes to be specified. It turns out that such an approach makes the problem too computationally expensive to solve when the apertures are small compared to the conductor area.

Alternatively, the approach we employed here is the EFIE-MFIE hybrid method. Imposing the equivalence principle, we are allowed to close the apertures with perfect conductor sheets, and then place a pair of magnetic current sheets in the hole region. The resulting magnetic current is defined as

$$\mathbf{M}(\mathbf{r}) = \mathbf{E}(\mathbf{r}) \times \hat{\mathbf{n}} \tag{3}$$

Thus the problem has become that of finding the electric currents on the signal lines above a solid perfect ground, and the magnetic currents above the aperture area. Applying image theory, the ground plane is removed, with its effect replaced by the images of the electric current and magnetic current. Based on this approach, the free space dyadic Green's functions can be used.

In an manner similar to the EFIE formulation, on the conductor surface, we have

$$\{\mathbf{E}_e(\mathbf{J}) + \mathbf{E}_m(\mathbf{M})\} \times \hat{\mathbf{n}} = 0 \tag{4}$$

The electric field induced by magnetic current sources is

$$\mathbf{E}_m(\mathbf{r}) = \int \bar{\mathbf{G}}_{Em}(\mathbf{r},\mathbf{r}') \cdot \mathbf{M}(\mathbf{r}')dv' \tag{5}$$

where $\bar{\mathbf{G}}_{Em}$ are the dyadic Green's function (whose forms will be provided later in this section).

For a ground plane of zero thickness, the tangential components of the magnetic fields are continuous across the boundary in the aperture region. As a result, we arrived at the magnetic field integral equation

$$\hat{\mathbf{n}} \times [\mathbf{H}_e(\mathbf{J}) + \mathbf{H}_m(2\mathbf{M})] = 0 \tag{6}$$

where $\mathbf{M}$ denotes the magnetic current above the apertures. These magnetic fields can be computed by the corresponding integrals, involving the corresponding dyadic Green's functions. The four dyadic Green's functions are

$$\mathbf{H}_e(\mathbf{r}) = \int \bar{\mathbf{G}}_{He}(\mathbf{r},\mathbf{r}') \cdot \mathbf{J}(\mathbf{r}')dv' \tag{7}$$

$$\mathbf{H}_m(\mathbf{r}) = -j\omega\epsilon \int \bar{\mathbf{G}}_{Hm}(\mathbf{r},\mathbf{r}') \cdot \mathbf{M}(\mathbf{r}')dv' \tag{8}$$

where $\bar{\mathbf{G}}_{He}$ and $\bar{\mathbf{G}}_{Hm}$ are the free space dyadic Green's functions. The four dyadic Green's functions are

$$\bar{\mathbf{G}}_{Ee}(\mathbf{r},\mathbf{r}') = \bar{\mathbf{G}}_{Hm}(\mathbf{r},\mathbf{r}') = (\bar{\mathbf{I}} + \frac{1}{k^2}\nabla\nabla)g(\mathbf{r},\mathbf{r}') \tag{9}$$

$$\bar{\mathbf{G}}_{He}(\mathbf{r},\mathbf{r}') = \bar{\mathbf{G}}_{Em}(\mathbf{r},\mathbf{r}') = \nabla \times \bar{\mathbf{G}}_{Ee}(\mathbf{r},\mathbf{r}') \tag{10}$$

where

$$g(\mathbf{r},\mathbf{r}') = \frac{e^{-jk|\mathbf{r}-\mathbf{r}'|}}{4\pi|\mathbf{r}-\mathbf{r}'|} \tag{11}$$

In the previous equations the first subscript denotes the type of field, while the second denotes the type of source. The effect of the ground plane is taken into account by including the contribution of the image currents.

B. Spectral Domain Representation of Currents and Fields

Consider a two-dimensional structure as shown in Fig. 1 in which the structure is periodic with period Λ_x and Λ_y in x and y direction, respectively. By using the Floquet theorem, the electric current can be written as

$$\mathbf{J}(x,y,z)=\sum_{n=-\infty}^{\infty}\sum_{m=-\infty}^{\infty}\mathbf{J}_{nm}(z)e^{j(\kappa_{xn}x+\kappa_{ym}y)} \tag{12}$$

with $\kappa_{xn}=p_{xn},\kappa_{ym}=p_{ym}+k_{y0}$, $p_{xn}=\frac{2n\pi}{\Lambda_x}$, and $p_{ym}=\frac{2m\pi}{\Lambda_y}$. k_{y0} is the propagation constant in y direction, and $\mathbf{J}_{nm}(z)$ is the Fourier coefficients given by

$$\mathbf{J}_{nm}(z)=\frac{1}{\Lambda_x\Lambda_y}\int_0^{\Lambda_x}\int_0^{\Lambda_y}\mathbf{J}(x,y,z)e^{-j(p_{xn}x+p_{ym}y)}dxdy \tag{13}$$

which is a function of spatial coordinate z only. Similarly we can represent $\mathbf{M}(x,y,z)$ by Fourier series.

To find the spectral domain representation of the fields, we first give the spectral domain representation of the Green's function. For two-dimensional periodic structures, we have

$$\hat{g}(z-z',\kappa_{xn},\kappa_{ym})=\int\int g(\mathbf{r},\mathbf{r}')e^{j[\kappa_{xn}(x'-x)+\kappa_{ym}(y'-y)]}dx'dy' \tag{14}$$

which has a closed form as

$$\hat{g}(z-z',\kappa_{xn},\kappa_{ym})=\frac{e^{-j\kappa_{znm}|z-z'|}}{j2\kappa_{znm}} \tag{15}$$

where

$$\kappa_{znm}=\sqrt{k_0^2-\kappa_{xn}^2-\kappa_{ym}^2} \tag{16}$$

If the structure is periodic only in the propagation direction, we have

$$\tilde{g}(x-x',z-z',k_{ym})=\frac{1}{4\pi}\sqrt{\frac{2}{\pi}}K_0(\rho\sqrt{k_{ym}^2-k^2}) \tag{17}$$

where $K_0(\rho\sqrt{k_{ym}^2-k_2})$ is the modified Bessel function, and

$$\rho=\sqrt{(x-x')^2+(z-z')^2} \tag{18}$$

For simplicity, in the following derivation we only discuss the two-dimensional periodic case, the one dimensional case can be obtained very easily in a similar fashion. For convenience, we define $\tilde{G}_0$ as

$$\tilde{G}_0(x,y,z,z',n,m)=\hat{g}(z-z',\kappa_{xn},\kappa_{ym})e^{j(\kappa_{xn}x+\kappa_{ym}y)} \tag{19}$$

By defining $\theta_{nm}=\kappa_{xn}x+\kappa_{ym}y-\kappa_{znm}|z-z'|$, where θ_{nm} is a function of x,y,z,z' and also of κ_{xn} and κ_{ym}, we have

$$\tilde{G}_0(x,y,z,z',n,m)=\frac{e^{j\theta_{nm}}}{j2\kappa_{znm}} \tag{20}$$

The fields induced by the electric and magnetic sources are obtained in the following form

$$\mathbf{E}_e(x,y,z)=\sum_{nm}\int\bar{\mathbf{Z}}_{nm}\cdot\mathbf{J}_{nm}(z')e^{j\theta_{nm}}dz' \tag{21}$$

$$\mathbf{E}_m(x,y,z)=\sum_{nm}\int\bar{\mathbf{T}}_{nm}^{Em}\cdot\mathbf{M}_{nm}(z')e^{j\theta_{nm}}dz' \tag{22}$$

$$\mathbf{H}_e(x,y,z)=\sum_{nm}\int\bar{\mathbf{T}}_{nm}^{He}\cdot\mathbf{J}_{nm}(z')e^{j\theta_{nm}}dz' \tag{23}$$

$$\mathbf{H}_m(x,y,z)=\sum_{nm}\int\bar{\mathbf{Y}}_{nm}\cdot\mathbf{M}_{nm}(z')e^{j\theta_{nm}}dz' \tag{24}$$

where $\bar{\mathbf{Z}}_{nm},\bar{\mathbf{T}}_{nm}^{Em},\bar{\mathbf{T}}_{nm}^{He}$ and $\bar{\mathbf{Y}}_{nm}$ are 3×3 tensors. The tensor elements of $\bar{\mathbf{Z}}$ and $\bar{\mathbf{Y}}$ are obtained as

$$Z_{\alpha\beta nm}=\frac{\omega\mu}{2k_0^2}\frac{\kappa_\alpha\kappa_\beta}{\kappa_{znm}},Y_{\alpha\beta nm}=\frac{\omega\epsilon}{2k_0^2}\frac{\kappa_\alpha\kappa_\beta}{\kappa_{znm}} \tag{25}$$

where $\{\alpha,\beta=x,y,z\}$, $\alpha\neq\beta$, and

$$Z_{\alpha\alpha nm}=-\frac{\omega\mu}{2k_0^2}\frac{(k_0^2-k_\alpha^2)}{\kappa_{znm}},\quad Y_{\alpha\alpha nm}=-\frac{\omega\epsilon}{2k_0^2}\frac{(k_0^2-k_\alpha^2)}{\kappa_{znm}} \tag{26}$$

where $\alpha=x,y$, and

$$Z_{zznm}=-\frac{\omega\mu}{2k_0^2}\frac{(k_0^2-k_{znm}^2)-j2\kappa_{znm}\delta(z-z')}{\kappa_{znm}} \tag{27}$$

$$Y_{zznm}=-\frac{\omega\epsilon}{2k_0^2}\frac{(k_0^2-k_{znm}^2)-j2\kappa_{znm}\delta(z-z')}{\kappa_{znm}} \tag{28}$$

In the previous equations the use of the relation has been made

$$\frac{d}{dz}sgn(z-z')=2\delta(z-z') \tag{29}$$

where $sgn(z)$ is the sign function.

The tensor elments of $\bar{\mathbf{T}}^{Em}$ and $\bar{\mathbf{T}}^{He}$ are obtained as

$$T_{\alpha\alpha nm}^{Em}=T_{\alpha\alpha nm}^{He}=0 \tag{30}$$

where $\alpha=x,y,z$, and

$$\begin{cases}T_{xynm}^{Em}=T_{yxnm}^{He}=-T_{yxnm}^{Em}=-T_{xynm}^{He}=-\frac{1}{2}sgn(z-z')\\ T_{xznm}^{Em}=T_{zxnm}^{He}=-T_{zxnm}^{Em}=-T_{xznm}^{He}=-\frac{\kappa_{ym}}{2\kappa_{znm}}\\ T_{yznm}^{Em}=T_{zynm}^{He}=-T_{zynm}^{Em}=-T_{yznm}^{He}=\frac{\kappa_{xn}}{2\kappa_{znm}}\end{cases} \tag{31}$$

Thus we get the final form of the combined integral equations as

$$\hat{\mathbf{n}}\times\sum_{nm}\int\{\bar{\mathbf{Z}}_{nm}\cdot\mathbf{J}_{nm}(z')+\bar{\mathbf{T}}_{nm}^{Em}\cdot\mathbf{M}_{nm}\}e^{j\theta_{nm}}dz'=0 \tag{32}$$

$$\hat{\mathbf{n}}\times\sum_{nm}\int\{\bar{\mathbf{T}}_{nm}^{He}\cdot\mathbf{J}_{nm}(z')+\bar{\mathbf{Y}}_{nm}\cdot\mathbf{M}_{nm}\}e^{j\theta_{nm}}dz'=0 \tag{33}$$

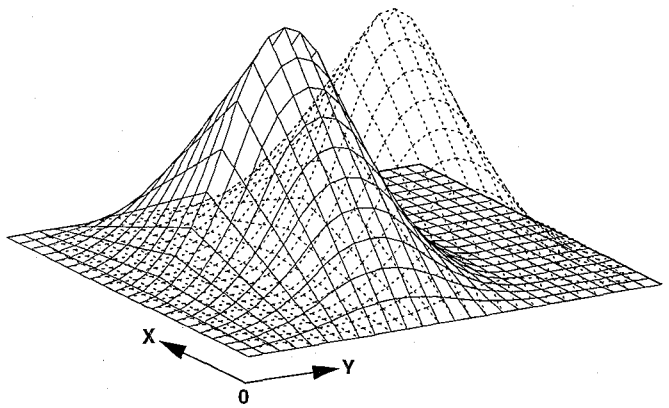

Fig. 2. Two-dimensional spline basis, first order in x direction and second order in y direction. Solid line: $b(x,y) = B_1(x)B_2(y)$; dashed line: $b(x,y-1) = B_1(x)B_2(y-1)$.

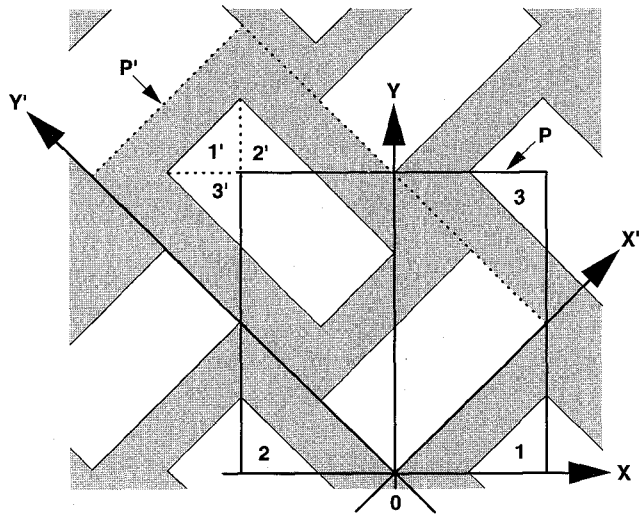

Fig. 3. Redefined period and coordinate rotation: rectangular apertures.

III. Numerical Solution of Integral Equations

A. Expansion of Currents with Piecewise Basis

As a first step in the numerical solution, we expand the surface current by means of a set of basis functions, yielding

$$|J_\alpha(x,y,z)\rangle = [B^e_\alpha]|J_\alpha\rangle \tag{34}$$

$$|M_\alpha(x,y,z)\rangle = [B^m_\alpha]|M_\alpha\rangle \tag{35}$$

where $\{\alpha = x,y,z\}$ respectively; $\{b^\beta_{\alpha i}(x,y,z),\ \alpha = x,y,z,\beta = e,m\}$ are the $i-th$ basis function for the six current components. It follows that the Fourier transform of the currents is obtained as

$$|J_{\alpha nm}(z)\rangle = \left[\hat{B}^e_{\alpha nm}\right]|J_\alpha\rangle \tag{36}$$

$$|M_{\alpha nm}(z)\rangle = \left[\hat{B}^m_{\alpha nm}\right]|M_\alpha\rangle \tag{37}$$

where $\hat{B}^\beta_{\alpha nm}(z)$ are the Fourier transform of the basis functions $\{b^\beta_{\alpha nm}(z), \alpha = x,y,z,\beta = e,m\}$.

If only the surface currents are considered, the volume current degenerates to a surface current distribution. Thus the basis functions are defined on surfaces, and in this paper the basis functions are defined in rectangular patches. Using local coordinates, for convenience, the basis functions have the following form

$$B_{u\alpha} = P(u-u_{u\alpha})T(v-v_{u\alpha})\delta(w-w_{u\alpha}) \tag{38}$$

where v and u are respectively the direction of the current flow and the transverse direction, w is the normal direction to the conductor surface.

As discussed before, both fields and currents are represented in the form of two dimensional Fourier series. The convergence of the series is a very important factor in numerical computations. To achieve a rapid convergence rate, a smooth basis should be used. In this article, the B-spline functions of different orders are used for functions $P(u)$ and $T(v)$.

A B-spline function of N-th order is defined as

$$B_N(x) = B_{N-1}(x) * B_0(x) \tag{39}$$

where $*$ denotes the convolution operator, and $B_N(x)$ has a compact support of $[0, N+1]$, that is, it is nonzero only within $[0, N+1]$. The commonly used pulse function and triangle functions are the simplest B-spline functions of order 0 and order 1. A third order B-spline function has the following form

$$B_3(x) = \frac{1}{6}\sum_{l=0}^{4}\binom{4}{l}(-1)^l(x-l)^3_+ \tag{40}$$

where

$$(x-l)_+ = \begin{cases} x-l & if\ \ x \geq l \\ 0 & otherwise \end{cases} \tag{41}$$

The Fourier transform of the B-spline functions takes the form

$$\hat{B}_N(\omega) = \left(\frac{1-e^{-j\omega}}{j\omega}\right)^{N+1} \tag{42}$$

It may be noted that we can increase the rate of convergence of the double Fourier series by increasing the smoothness of the basis functions. However since the high order splines take more spatial support, a finer discretization is needed. An effect way to avoid this problem is using higher order splines in the current direction, while using lower order splines for the other direction. An example of hybrid spline basis is shown in Fig. 2.

B. Galerkin's Method and Matrix Equation

Substituting (36), (37) into (32), (33), we have

$$\sum_{nm}\int \hat{\mathbf{n}}\times\left\{\bar{\mathbf{Z}}_{nm}\cdot\begin{bmatrix}[B^e_x][J_x]\\ [B^e_y][J_y]\\ [B^e_z][J_z]\end{bmatrix} + \bar{\mathbf{T}}^{Em}_{nm}\cdot\begin{bmatrix}[B^m_x][M_x]\\ [B^m_y][M_y]\\ [B^m_z][M_z]\end{bmatrix}\right\} e^{j\theta_{nm}}dz' = 0 \tag{43}$$

$$\sum_{nm}\int \hat{\mathbf{n}}\times\left\{\bar{\mathbf{T}}^{He}_{nm}\cdot\begin{bmatrix}[B^e_x][J_x]\\ [B^e_y][J_y]\\ [B^e_z][J_z]\end{bmatrix} + \bar{\mathbf{Y}}_{nm}\cdot\begin{bmatrix}[B^m_x][M_x]\\ [B^m_y][M_y]\\ [B^m_z][M_z]\end{bmatrix}\right\} e^{j\theta_{nm}}dz' = 0 \tag{44}$$

which are two sets of linear equations with finite number of unknowns. By choosing the weighting functions in the same

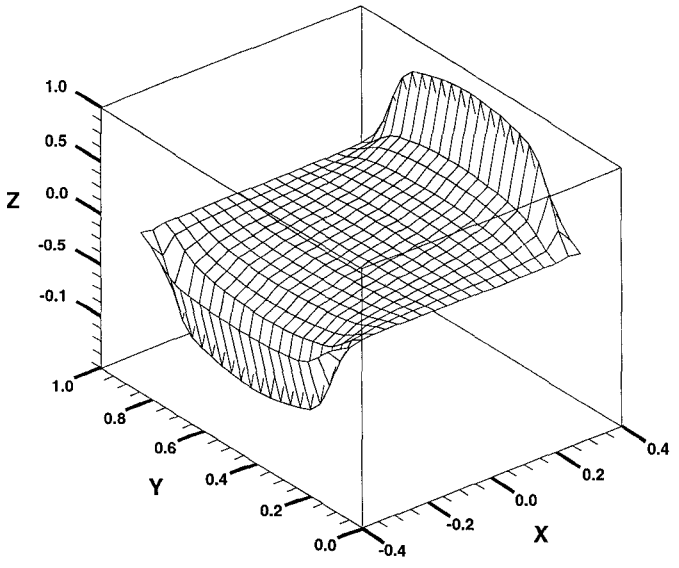

Fig. 4. x-component of electrical field in the aperture, by EFIE-MFIE hybrid method.

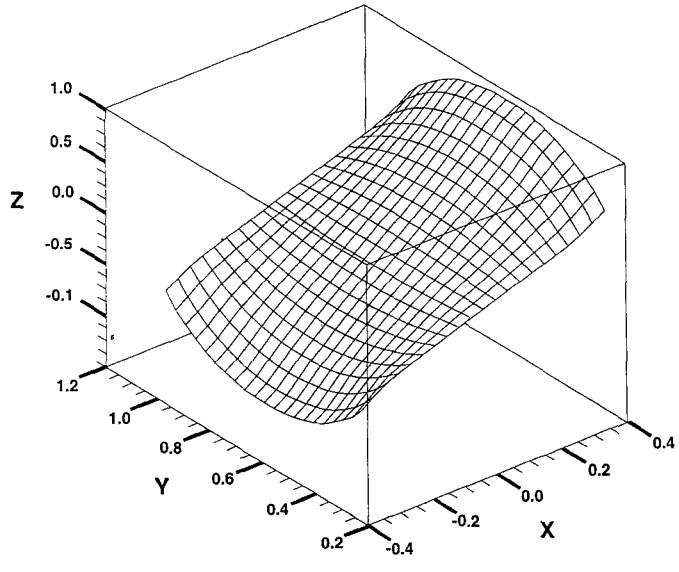

Fig. 5. x-component of electrical field in the aperture, by EFIE method.

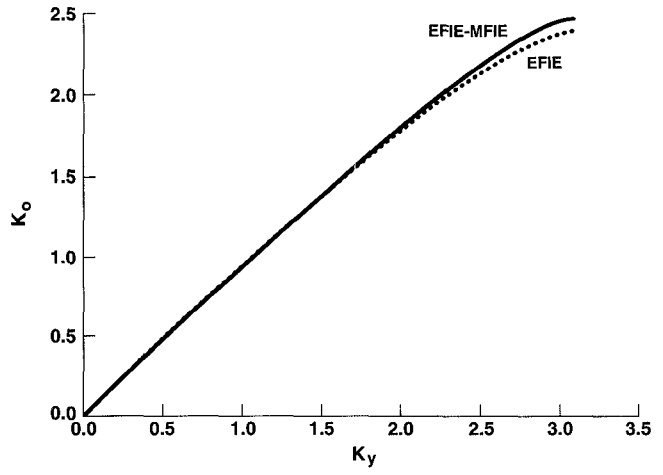

Fig. 6. Comparison of dispersive characteristics between EFIE-MEIE hybrid method and EFIE method.

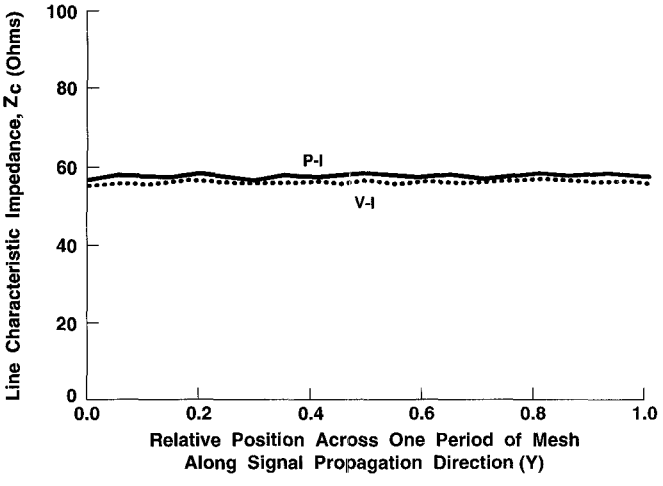

Fig. 7. Comparison of impedance between P-I and V-I definitions.

way as the set of basis functions, we have a Galerkin solution for the combined field integral equations

$$\begin{bmatrix} \begin{bmatrix} Z^{Ee}_{\alpha\beta} \end{bmatrix} & \begin{bmatrix} T^{Em}_{\alpha\beta} \end{bmatrix} \\ \begin{bmatrix} T^{He}_{\alpha\beta} \end{bmatrix} & \begin{bmatrix} Y^{Mm}_{\alpha\beta} \end{bmatrix} \end{bmatrix} \begin{bmatrix} [J_\beta] \\ [M_\beta] \end{bmatrix} = [0] \tag{45}$$

where $\alpha, \beta = x, y, z$, each of the four submatrices is a 3×3 submatrix with the matrix elements as

$$[X_{\alpha\beta}]_{ij} = \sum_{nm} \iint \bar{\mathbf{X}}_{\alpha\beta nm} \hat{B}^e_{\alpha,i}(p_{xn}, p_{ym})$$

$$\hat{B}^e_{\beta,j}(\kappa_{xn}, \kappa_{ym}) e^{-j\kappa_{znm}|z-z'|} dz' dz \tag{46}$$

where $X = Z, T^{Em}, T^{He}$ and Y, $\bar{\mathbf{X}} = \bar{\mathbf{Z}}, \bar{\mathbf{T}}^{Em}, \bar{\mathbf{T}}^{He}$ and $\bar{\mathbf{Y}}$, $\alpha, \beta = x, y, z$.

By enforcing the determinant of the coefficient matrix of (45) to zero, we will solve for the propagation constant k_y, and furthermore, for the eigen current and field distributions.

C Expansion of Magnetic Currents and Coordinate Rotation

Though the ground plane is periodically perforated with rectangular apertures, the periodicity of the structure depends on the orientation of the signal lines. Λ_x,Λ_y, the period of the structure in x and y direction, are determined by $tan\theta = \frac{\Lambda_y}{\Lambda_x}$, which must be an rational number. Since a rational number is defined by the ratio of two integers, Λ_x, Λ_y are the corresponding minimal integral numerator and denominator, respectively. Fig. 1 depicts the case in which the angle between the aperture edge and the signal line is θ. When $\theta = 0$, we obtain a parallel problem similar to that of [6]; when $\theta = 45^o$, we get a structure in which the signal lines are in the diagonal direction of the apertures. Note that the basis functions are defined on rectangular cells. For the structures in Fig. 3, one problem with the Fourier series expansion of the current is that some basis functions are divided into different periods, where each period is usually defined as a rectangular

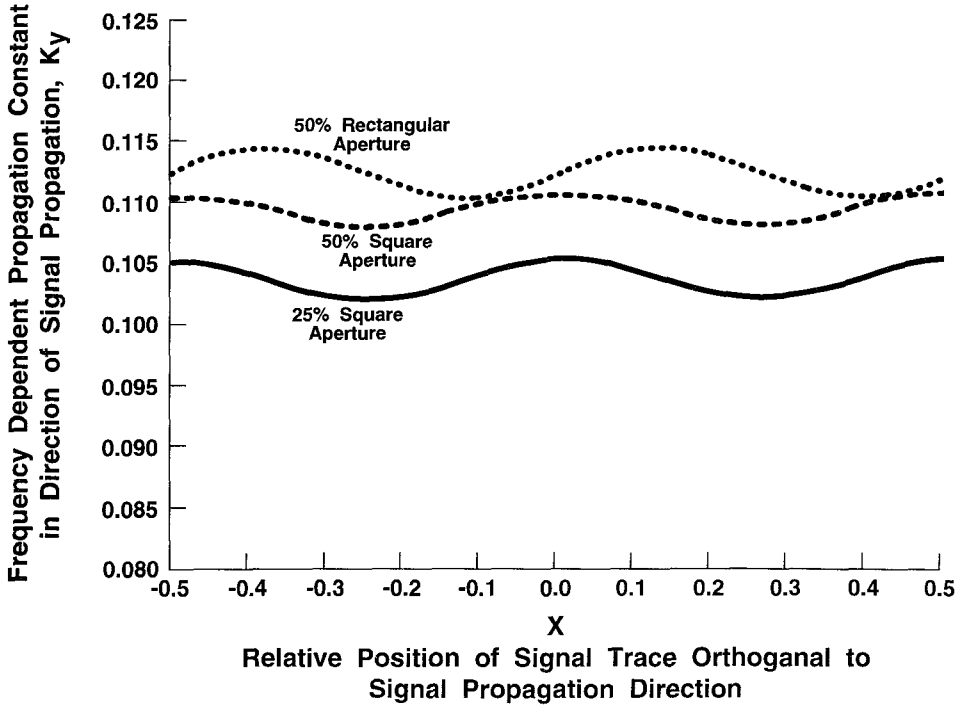

Fig. 8. Propagation constant k_y versus x, 25% square, 50% square, and 50% rectangular apertures, 45° case.

cell, as shown in Fig. 3. This problem can be circumvented by utilizing the periodicity of the Fourier transform and the periodicity of the structure, that is, to rearrange the unit cell as shown in the rectangular bordered by dashed lines, and referenced to the (x', y') coordinates. Mathematically the old and new unit cells are equivalent.

Consider the general structure in Fig. 1, where the angle between the signal line and the edge of aperture in the ground is denoted as θ. In (x, y) coordinates, the x and y components of the magnetic current are obtained by expanding them in the (x', y') coordinate in terms of basis functions,

$$M_x = \sum_{i=1}^{N_x^m} M_{x'i} b_{x'i}^m cos\theta - \sum_{i=1}^{N_y^m} M_{y'i} b_{y'i}^m \sin\theta \tag{47}$$

$$M_y = \sum_{i=1}^{N_x^m} M_{x'i} b_{x'i}^m sin\theta + \sum_{i=1}^{N_y^m} M_{y'i} B_{y'i} \cos\theta \tag{48}$$

where

$$x = x'\cos\theta - y'\sin\theta \qquad y = x'\sin\theta + y'\cos\theta \tag{49}$$

then Fourier coefficients of M_x and M_y are

$$\begin{bmatrix} M_{xnm} \\ M_{ynm} \end{bmatrix} = \begin{bmatrix} \cos\theta & -\sin\theta \\ \sin\theta & \cos\theta \end{bmatrix} \begin{bmatrix} M_{x'nm} \\ M_{y'nm} \end{bmatrix} \tag{50}$$

where

$$M_{x'nm} = \sum_{i=1}^{N_x^m} \int\int_{S'} M_{x'i} b_{x'i}^m e^{-j(p'_{xnm}x' + p'_{ynm}y')} dx'dy' \tag{51}$$

$$M_{y'nm} = \sum_{i=1}^{N_y^m} \int\int_{S'} M_{y'i} b_{y'i}^m e^{-j(p'_{xnm}x' + p'_{ynm}y')} dx'dy' \tag{52}$$

where $p_{x'nm}, p_{y'nm}$ are defined as $p'_{xnm} = p_{xn}\cos\theta + p_{ym}\sin\theta$, $p'_{ynm} = -p_{xn}\sin\theta + p_{ym}\cos\theta$.

D. Convergence of the Fourier Series

The numerical solution involves the calculation of the two dimensional summations which are truncated at some lengths that are determined by the convergence rate of the series. Denoting the convergence rate of the basis function as $N_u \times N_v$,

$$|\hat{B}(p_{un}, p_{vm})| \sim \frac{1}{n^{N_u+1} m^{N_v+1}} \tag{53}$$

where N_u, N_v are the orders of the basis in dimensions u and v, and $(u, v) = (x, y)$ or (x', y'), then the convergence rate of each element is in the order of $4(N_u + 1) \times (N_v + 1)$ for the Galerkin solution.

Rigorously speaking, (53) only gives the asymptotic convergence property of the series. Besides the rate of convergence, the length of the summation for the given accuracy also depends on the size of the geometry. If the discretization size is too small, a longer truncation is needed.

One problem with the coordinate rotation is the convergence behavior of the two dimensional Fourier series. Note that the basis functions are defined in the source region while the testing functions are defined in the field region. They may be defined in the primed and unprimed coordinate systems, respectively, and their Fourier transform, in this case, will be the functions of p_{xn}, p_{ym} and p'_{xnm}, p'_{ynm}, or $n, m, n +$

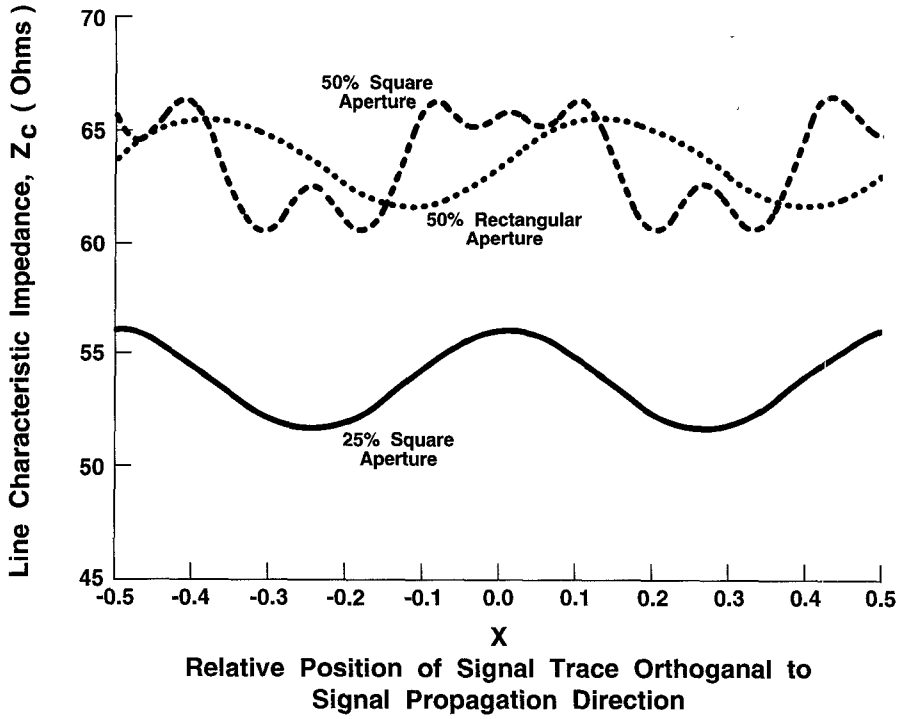

Fig. 9. Impedance Z_c versus x, 25% square, 50% square, and 50% rectangular apertures, 45° case.

$m, n-m$ if $\theta = 45^o$. As a result, the rate of convergence may not be as high as estimated above. Fortunately, this case only occurs for the interaction between the signal line and the ground aperture, there is an exponentially decaying factor associated with $|z-z'|$, which makes the series converge very rapidly.

IV. Equivalent Transmission Line Model and Characteristic Impedance

Given the fact that the structure has discontinuities in the propagation direction, it is natural to conceive that the characteristic impedance is the function of the position along the line. It is true if we only consider the traveling wave. However, by solving the eigen equation in the last section, we obtained the propagation velocity and eigen current and field distributions for the dominant mode. This mode consists of the superposition of all spatial harmonics, each of them can not exist by itself except under some special circumstances such that the period is the multiples of the wavelength. As a consequence, there does not exists a pure traveling wave but a combination of the traveling waves and standing waves. Hence the characteristic impedance of the signal line is not uniquely defined [12].

However, if the working frequency is not extremely high so the period is smaller than the wavelength of interest, and the displacement current is much smaller than the conducting electric current, we can establish a uniform transmission line model from the fact that the propagation current is a constant along the signal line. The characteristic impedance of the equivalent transmission line can be defined either by the voltage-current definition or power-current definition [13]. As shown later later, these two definitions are consistent.

By letting the potential of the ground plane be zero, the voltage-current definition gives the characteristic impedance as

$$Z_c(y) = \frac{V(y)}{I(y)} \tag{54}$$

In the above equation $I(y)$ is the electric current flowing in the propagation direction on the signal line, which is a constant along the signal line and can be evaluated from

$$I(y) = \oint \mathbf{H}(x,y,z) \cdot d\mathbf{l} \tag{55}$$

while $V(y)$ is the electric potential of the signal line which is defined as

$$V(y) = \int_g^s \mathbf{E}(x,y,z) \cdot d\mathbf{l} \tag{56}$$

where g, s are the reference points at the ground and signal line, respectively. Since the electric potential in the aperture region is not zero, the reference point g should be chosen on the conductor part of the ground plane.

The power-current definition of the impedance is

$$Z_c = \frac{2P}{|I|^2} \tag{57}$$

where P is the average power associated with the eigenfields flowing through a period, and can be found as

$$P = \int_0^{\Lambda_x} dx \int_{-\infty}^{\infty} S_y dz \tag{58}$$

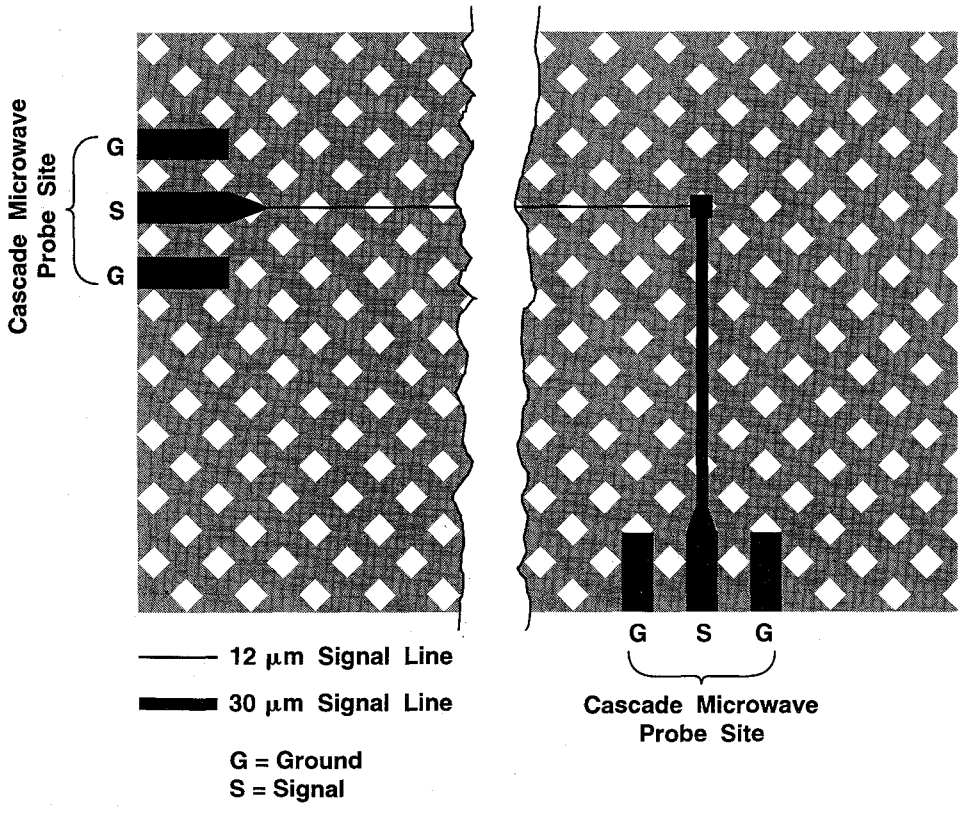

Fig. 10. Configuration of Boeing test coupon. Mesh ground plane is 40 μm pitch, 25% aperture. Probe pad size is $75 \times 100\,\mu m$, $150\,\mu m$pitch. Pads are arranged in G-S-G configuration, and electrically conected to signal lines and ground through vias.

where

$$S_y = \frac{1}{2} Re\{\mathbf{E} \times \mathbf{H}^*\} \cdot \hat{y} \tag{59}$$

the superscript $*$ denotes the complex conjugate.

From Eqs.(21)-(24), the Poynting vector takes the following form

$$S_y = \frac{1}{2} \sum_{nm} \sum_{n'm'} \{\mathbf{E}_{nm} \times \mathbf{H}^*_{n'm'}\} \cdot \hat{y} \tag{60}$$

where

$$\mathbf{E}_{nm} = \int \left(\bar{\mathbf{Z}}_{nm} \cdot \mathbf{J}(z') + \bar{\mathbf{T}}^{Em}_{nm} \cdot \mathbf{M}_{nm}\right) e^{j\theta_{nm}} dz' \tag{61}$$

$$\mathbf{H}_{nm} = \int \left(\bar{\mathbf{T}}^{He}_{nm} \cdot \mathbf{J}(z') + \bar{\mathbf{Y}}^{Em}_{nm} \cdot \mathbf{M}_{nm}\right) e^{j\theta_{nm}} dz' \tag{62}$$

From the orthogonality of trigonometric functions, the integration with respect to x in Eq.(58) will annihilate the summation with respect to n', and we obtained the expression for power as

$$P = \frac{\Lambda_x}{2} \sum_{nmm'} \int_{-\infty}^{\infty} \{\mathbf{E}_{nm} \times \mathbf{H}^*_{nm'}\} \cdot \hat{y} dz \tag{63}$$

V. Numerical Results and Measurements

As a numerical example, we first studied the structure in Fig. 1 with $\theta = 0$, in which the signal lines are oriented directly above the center of the apertures and parallel with the aperture edges. The normalized dimension of the structure has a period of 1 unit $\times 1$ unit with a 56.25% square aperture; the width and height of the signal lines are 0.25 and 0.5, respectively. This structure is also studied in [6] and [8] by means of the EFIE formulation. In this paper, the structure is solved by the hybrid EFIE-MFIE formulation. The x-component of electric field E_x in the aperture region is plotted in Fig. 4 from the hybrid method, and Fig. 5 from EFIE method. From these figures it may be observed that the EFIE approach results in significant numerical errors that lead to large nonzero tangential fields at the aperture edges. These nonzero fields make the effective aperture area appear larger than it should be. On the contrary, the hybrid solutions satisfy the boundary condition accurately, thus providing better results than does the EFIE method.

Fig. 6 compares the propagation constant obtained by the two methods: the solid line represents the result for the hybrid method and the dashed line for the EFIE method. At $k_0 = 0.01$, the EFIE generates the value of the propagation constant of the dominant mode of $k_y = 0.010683$, which is essentially the same as the result from the hybrid method. As the frequency increases, i.e. for larger k_0, the EFIE demonstrated a greater dispersion of the propagation constant with frequency than does the hybrid method, due to the larger effective aperture, which is inaccurate.

To verify the validity of the two definitions of the characteristic impedance given in the previous section, we computed the impedance of the structure as shown in Fig. 1 with $\theta = 45^o$. The signal lines in this structure are $12\,\mu m$ wide, $5\,\mu m$ thick, and $5\,\mu m$ above a perfect ground plan perforated with $40 \times 40\,\mu m$ square apertures; the line pitch is $80\,\mu m$. By

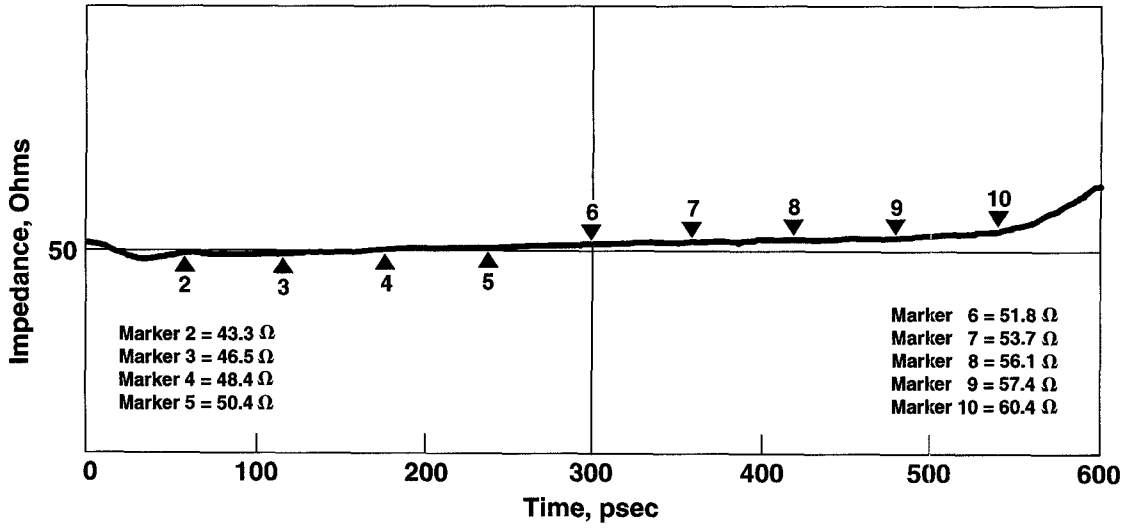

Fig. 11. TDR measurement of characteristic impedance on HP54123.

normalizing the period to 1×1, we converted the width and height of the signal line to 0.212132 and 0.088388. In principle, the formulae (32) and (33) are full wave equations, and can handle transmission lines of finite thickness. However, for simplicity, we ignored the thickness of the signal lines in the next few examples. After the eigencurrents and eigenfields are obtained, the characteristic impedance is evaluated by means of the voltage-current and power-current definitions. The results are illustrated in Fig. 7. It may be observed that the two definitions give approximately the same results. However, since the power-current definition involves triple summations, much more CPU time is required to achieve the result.

To study the variations of dispersion and impedance caused by the relative position x of the signal line with respect to the aperture , and the shape and size of the apertures, we calculate the propagation constant and characteristic impedance employing the EFIE-MFIE approach. The propagation characteristics and the characteristic impedance versus location x are shown in Figs. 8, 9, where the normalized wavenumber is chosen to be $k_0 = 0.1$, the aperture size is 25% and 50% for square apertures, and 50% for rectangular aperture, respectively.

The comparison of the propagation velocities of the signals for different structures are shown in Table I, where four cases are calculated. The width of the signal line is $12\,\mu m$, height to the ground is $5\,\mu m$, pitch-to-pitch distance is $80\,\mu m$, all with 50% aperture/period ratio. The working frequency is chosen at $5.9GHz$ which corresponds to $k_0 = 0.01$. The length of the Fourier series are chosen at $L_x = 16, L_y = 16$ and $L_x = 32, L_y = 32$, respectively, the results are accurate to the fifth digit. We can see that the location and shape of the aperture affect the dispersion greatly.

From the figures described above, we can see that dispersion and impedance depend on the percentage area of the conducting plane directly beneath the signal line. To reduce the variance of dispersion and impedance as functions of x, a rectangular aperture meshed ground plane is proposed in [14]. This proposal has been rigorously evaluated in this paper. The dispersion and impedance values versus location x for a rectangular aperture meshed ground plane, in which the dimension of the aperture is $\frac{\sqrt{2}}{2} \times \frac{\sqrt{2}}{4}$, as shown in Fig. 3. Comparing these results with the other curves in Figs. 8 and 9 we conclude, in contradiction to the claim in [14], that the rectangular aperture scheme slightly improves impedance but worsens dispersion over the square aperture scheme. Nonetheless, from the manufacturing perspective, particularly for correct alignment of through-hole vias, the rectangular scheme is much more difficult to fabricate with high yield.

To verify our numerical solutions, we measured the characteristic impedance of a meshed ground plane test coupon donated by the Boeing Aerospace Co. The measurements are conducted on both an HP-8510C network analyzer and on an HP-54123 sampling oscilloscope. Fig. 10 shows the configuration of one of the meshed ground plane test coupons designed and fabricated by the Boeing Aerospace Co., while the TDR measurement of the coupon from the HP 54123 is plotted in Fig. 11. Table II shows the comparison for different approaches. We can see from the table that when the finite thickness of the signal lines is incorporated into the simulations, the numerical results agree very well with the measurements.

VI. Conclusion

In this paper, the dyadic Green's function formulation is applied to derive a hybrid EFIE-MFIE method. The method can be easily extended to the analysis of multilyered structures [15],[16]. The B-spline functions are employed as the basis set. It is found that faster convergence can be achieved by an increase in the order of the splines. The method can also be adapted for the lossy conductor case. Several numerical examples are presented, and a real-world structure is analyzed. The effects of the location of signal lines, and the shape and size of the metal plane apertures on signal dispersion and line impedance are studied. Numerical results agreed well with the measurements.

v_c is the signal propagation velocity of a strip line above a solid ground plane.

TABLE I
COMPARISON OF SIGNAL PROPAGATION VELOCITY FOR DIFFERENT STRUCTURES

Parallel case	above conductor	$v_p/v_c = 0.9514$
	above aperture	$v_p/v_c = 0.8237$
Diagonal case	square	$v_p/v_c = 0.9058$
	rectangular	$v_p/v_c = 0.8901$

v_c is the signal propagation velocity of a strip line above a solid ground plane.

TABLE II
COMPARISON BETWEEN NUMERICAL RESULTS AND MEASUREMENTS

Models	***Impedence***	
Numerical Result	t=0	57.5Ω
	t=5μ m	53.4Ω
Measurement (Averaged)	HP8510C	52.0Ω
	HP54123	53.3Ω

ACKNOWLEDGMENT

The authors wish to thank Dr. J. Murphy, ARPA/ESTO, Dr. R. Pohanka and Dr. L. Kabacoff, ONR, and Dr. P. Young, Boeing Aerospace, for support and helpful discussions, and S. Richardson for assistance in the preparation of text and figures.

REFERENCES

[1] B. K. Gilbert and G. W. Pan, "Packaging of GaAs signal processors on multichip modules," *IEEE Trans. on Components, Hybrids, and Manufacturing Technol.*, vol. 15, no. 1, pp. 15–28, Feb. 1992.

[2] G. Pan, K. Olson, and B. Gilbert, "Frequency-domain solution for coupled stripline with crossing strips," *IEEE Trans. Microwave Theory Tech.* vol. MTT-39, no. 6, pp. 1013–1017, June 1991.

[3] G. Pan, G. Wunsch, and B. Gilbert, "Frequency-domain analysis of coupled nonuniform transmission lines using Chebyshev pseudo-spatial techniques," *IEEE Trans. Microwave Theory Tech.*, vol. MTT-40, pp. 2025–2033, Nov. 1992.

[4] G. Pan, G. Wang, and B. Gilbert, "Analysis of nonlinear termination networks for coupled lossy and dispersive transmission lines," *IEEE Trans. Microwave Theory Tech.*, vol. MTT-41, no. 3, pp. 531–535, Mar. 1993.

[5] G. Pan, J. Tan, and J. Murphy, "Full-wave analysis of microstrip floating line discontinuities," *IEEE Trans. Electromagnetic Compatibility,* Feb. 1994.

[6] B. Rubin and H. Bertoni, "Waves guided by conductive strips above a periodical perforated ground plane," *IEEE Trans. Microwave Theory Tech.* vol. MTT-31, no. 7, pp. 541–549, July 1983.

[7] B. J. Rubin, "The propagation characteristics of signal lines in a mesh-plane environment," *IEEE Trans. Microwave Theory Tech.* vol. MTT-32, No. 5, pp. 522–531, May 1984.

[8] C. H. Chan and R. Mittra, "The propagation characteristics of signal lines embedded in a multilayered structure in the presence of a periodically perforated ground plane," *IEEE Trans. Microwave Theory Tech.*, vol. MTT-36, No. 6, pp. 968–975, June 1988.

[9] O. Shimada *et al.*, "Electrical properties of a multilater thin film substrate for multichip packages," in *IEEE/CHMT'89, IEMT Symp.*, Japan, 1989, pp. 121–127.

[10] M. J. D. Powell, *Approximation Theory and Methods.* Cambridge, UK: Cambridge University Press, 1981.

[11] M. Gribbons, A. Cangellaris, and J. Prince, "Finite-difference time domain analysis of pulse propagation in multichip module interconnects," *IEEE Trans. Components, Hybrids, and Manufacturing Technology*, vol. 16, no. 5, pp. 490–498, Aug. 1993.

[12] R. E. Collin, *Field Theory of Guided Waves.* New York: IEEE Press, 1991.

[13] J. R. Brews, "Transmission line models for lossy waveguide interconnections in VLSI," *IEEE Trans. Electron Devices*, vol. ED-33, No. 9, pp. 1356–1365, Sept. 1986.

[14] A. Sasaki and Y. Shimada, "Electrical design technology for low dielectric constant multilayer ceramic substrate," *IEEE Trans. Components, Hybrids and Manufacturing Technol.*, vol. 15, no. 1, pp. 56–62, Feb. 1992.

[15] J. F. Kiang ,S. M. Ali and J. A. Kong, "Propagation properties of striplines periodically loaded with crossing strips," *IEEE Trans. Microwave Theory Tech.*, vol. MTT-37, N0. 4, pp. 776–786, Apr. 1989.

[16] W. C. Chew, *Waves and Fields in Inhomogeneous Media.* New York: Van Nostrand-Reinhold, 1990.

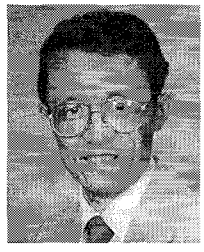

Guangwen Pan (S'81–83–M'84–SM'94) received the B.E. degree in mechanical engineering from Peking Institute of Petroleum Technology in 1967. He attended the Graduate School, University of Science and Technology of China from 1978 to 1980, majoring in electrical engineering. He received the M.S. degree in 1982, and the Ph.D. degree in 1984, both in electrical engineering from the University of Kansas, Lawrence, KS.

He worked at the Institute of R&D in Northwest of China in machine design as an associate engineer, and then as an electrical engineer responsible for design of pulse-width modulation electronics and digital remote fire control systems used in petroleum seismic exploration. He came to the United States in August 1980 as a research assistant in the Remote Sensing Laboratory, University of Kansas. From September 1984 to May 1985, he was a post-doctoral Fellow at the University of Texas, engaged in a project on computer-aided design of airborne antenna/radome systems. He joined the Mayo Foundation in 1985, engaged in the theoretical modeling of electromagnetic behavior of high-speed integrated circuits and systems, and placement and routing. From 1986 to 1988 he was an associate professor in the department of EE, South Dakota State University. In 1988 he joined the department of EECS at the University of Wisconsin-Milwaukee as an associate professor. He has been the Director of the Signal Propagation Research Laboratory since 1990 and became a professor in 1993. His research interests continue to be in the mathematical modeling of the electromagnetic environment of high clock rate signal processors.

Dr. Pan is a member of Eta Kapa Nu and is cited in *Who's Who in the Midwest* and *Who's Who in America*, and is on the Editorial Board of the IEEE TRANSACTIONS ON MICROWAVE THEORY AND TECHNIQUES.

Xiaojun Zhu (S'93) was born in Shandong Province, China, on July 9, 1963. He received the B.S. degree in radio electronic science from Shandong University and the M.S. degree in electrical engineering from Nanjing Institute of Posts and Telecommunications, China, in 1983 and 1988, respectively, and the Ph.D. degree in electrical engineering in the Department of EECS at the University of Wisconsin-Milwaukee, in May 1994.

From 1983 to 1985 he worked as an associate engineer in the Radar Department, Changhong Machinery Factory, Wuhan, China, on the calibration and measurement of radar antennas and feeding systems. From 1988 to 1990 he was on the faculty of the Department of Radio Engineering, Nanjing Institute of Posts and Telecommunications, Nanjing, China, where he was involved in the analysis, simulation and design of antenna and microwave components, and teaching of electromagnetic engineering. From 1990 to 1994 he was a graduate research assistant in the Signal Propagation Research Laboratory in the department of EECS, at University of Wisconsin–Milwaukee. His current research interests are electromagnetic modeling, analysis, and design of microwave circuits and components, interconnects and packaging of high speed VLSI and microelectronic systems. Currently, he is an engineer at Ansoft Corp.

Barry K. Gilbert (S'62–SM'87) received the B.S. in electrical engineering from Purdue University, Lafayette, IN, in 1965, and the Ph.D. in physiology and biophysics with minors in applied mathematics and electrical engineering, from the University of Minnesota, Minneapolis, in 1972.

He is presently a staff scientist and professor in the Department of Physiology and Biophysics, Mayo Foundation, Rochester, Minnesota. His research interests include the design of special-purpose computers for high-speed signal processing, and the development of advanced integrated circuit and electronic packaging technologies to support real-time signal processing of extremely widebanded data. He has worked on a variety of projects, including the development in the mid-1970's of a very wideband special-purpose data handling and array processing computer fabricated entirely with subnanosecond emitted coupled logic, and a special-purpose multiple instruction, multiple data (MIMD) processor capable of operating with up to 30 coprocessors under parallel microcode control in the late 1970's. He is currently responsible for the development of CAD tools at the system and integrated circuit levels, as well as high density electronic packaging technologies, to allow the fabrication of signal processing modules operation and gigahertz clock rate using GaAs digital integrated circuits and modules.